

## Preparation and Study of the Optical Properties of Poly (3-hexylthiophene-Co-thiophene) @NPs (SiO<sub>2</sub> , ZnO , Ag)

Ahmed Ismael

Hussein F. Hussein

Salah S. Al-luaibi\*

Physics Department, College of Education for Pure Sciences, Basrah University

\* Chemistry department, College of Science, Basrah University

### Abstract:

The study explores enhancing the optical of hybrid polymers by incorporating Poly(3HT-co-Thio)@NP (SiO<sub>2</sub>, ZnO, Ag ) into photo-electro-active layers useful in solar cell applications. These materials were examined and analysed using various techniques like X-ray diffraction (XRD), scanning electron microscopy (SEM), Fourier transform infrared spectroscopy (FTIR), Atomic Force Microscopy (AFM), and UV-visible Absorption Spectrum.

XRD analysis revealed high crystallinity in Poly(3HT-co-Thio)@SiO<sub>2</sub>, ZnO and Ag, with crystallite sizes between 70–80 nm. UV-visible absorption tests indicated band gap values of 1.78 eV, 1.82 eV, and 1.75 eV for SiO<sub>2</sub>, ZnO and Ag respectively the synthesized nanoparticles.

The polymeric membrane exhibited varying thicknesses of approximately 10.2 nm, 15.4 nm, and 155 nm, with surface roughness values of 5.19 nm, 6.48 nm, and 73.9 nm for SiO<sub>2</sub>, ZnO and Ag respectively of the polymer films. Analysis revealed a range of less than 100 nm for Poly(3HT-co-Thio)@SiO<sub>2</sub> and ZnO, measuring 63.3 nm due to agglomeration. Additionally, the polymer film on the nanoparticles varied in thickness from 5nm to 19 nm, indicating a thin, transparent layer capable of efficiently transmitting light.

**Keywords:** Poly(3HT-co-Thio)@NPs (SiO<sub>2</sub>,ZnO,Ag),Optical properties ,Nano particles.

### Introduction

Poly(3-hexylthiophene) (P3HT) materials have been Significantly studied for Their uses in organic optoelectronics. This is because it has high solubility in organic solvents and controllable crystallinity.[1]

Significant efforts have been made to develop the intrinsic properties of P3HT materials to enable their use in organic photovoltaic cells (OPVCs) [2].

When P3HT was used as a donor material in OPVCs hybrid polymers, in addition to the increase, it is necessary for the active organic layers in OPVCs to have good optical properties that help absorb solar energy with high efficiency [3].

Many researchers have reported tandem and hybrid structures with increased efficiency in absorbing sunlight in a wide spectral range [4].



Through the energy band gap, the optical properties of inorganic and organic nanostructures such as photoluminescence and absorption efficiency can be controlled through their shape, size and properties.

Crystal [5].

Various synthetic, processing and hybridization methods have been studied with different nanomaterials as a means of tuning the optical properties of polymeric nanostructures [6].

These manipulations are promising for tuning the optical properties of semiconducting organic polymeric nanoparticles (NPs) for application in OPVCs [7].

In this research, polymeric nanocomposites of P3HT were synthesized in aqueous suspension using additional polymerization [8]. To modify the optical properties, polymeric nanocomposites of P3HT were heat-treated in an aqueous suspension, i.e., compressed in a chamber at varying temperatures [9]. After heat treatment depending on different temperature, the ultraviolet and visible (UV/Vis) absorption spectra changed significantly with the intensity and width of the features [10].

There are two methods for preparing polymers: addition polymerization and condensation polymerization[11]. We used additive polymerization

## 2: Materials

**Various materials were sourced for this study:**

- 3-hexylthiophene with a 98%+ regioregularity and a molecular weight of 168.3 g/mol from Meryer (SHANGHAI) CHEMICAL TECHNOLOGY CO., LTD.
- Thiophene with a purity exceeding 99% from ORGANICS USA.
- PCBM from Ossila (UK) with a molar mass of 911 g/mol and purity surpassing 99%.
- PEDOT:PSS M 124-100ml variant from Ossila (UK).

**Nanoparticles used:**

- Silver Nano Particles (Ag NP) with 99.9% purity and an average size of 80nm from Hongwu International Group Ltd, China.
- Zinc Oxide Nano Particles (ZnO NP) with a size range of 20-30nm and 99.8% purity, also from Hongwu International Group Ltd.
- Silicon Dioxide Nano Particles (SiO<sub>2</sub> NP) with 99.5% purity and an average size of 20nm from Skyspring Nanomaterials, USA.

**All solvents utilized in this study were procured from Sigma-Aldrich.**

## 3: Experimental

### 3.1: synthesis of poly (3HT )

The synthesis of 3-hexylthiophene polymer involved several sequential steps. Initially, 0.84 grams of 3-hexylthiophene were mixed with a solution comprising 50 milliliters of CHCl<sub>3</sub>, and this mixture was degassed with nitrogen (N<sub>2</sub>) for approximately 5 minutes. Subsequently, 1.62 grams of iron chloride (FeCl<sub>3</sub>) were added to the degassed mixture, along with an additional 50



milliliters of  $\text{CHCl}_3$ , resulting in the formation of a slurry. The reaction mixture was stirred continuously for a period of 24 hours. After the stirring period, the mixture was introduced into 100 milliliters of methanol, causing the 3-hexylthiophene polymer to precipitate[12].

**3.2: Core shell polymerization of P3HT@NPs(  $\text{SiO}_2$ ,ZnO, Ag)**

In this experiment, a core-shell polymer nanocomposite was prepared using 3-hexylthiophene and a combination of  $\text{SiO}_2$  , ZnO , Ag nanoparticles. To initiate the synthesis, 0.84 grams of 3-hexylthiophene and an equivalent amount of the nanoparticles in a 1:4 ratio were combined. This mixture was then introduced to 50 milliliters of chloroform ( $\text{CHCl}_3$ ) and degassed with nitrogen ( $\text{N}_2$ ) for approximately 5 minutes under ultrasonic irradiation for half an hour[13]. Following degassing, 1.62 grams of ferric chloride ( $\text{FeCl}_3$ ) and an additional 50 milliliters of  $\text{CHCl}_3$  were added to create a slurry. The resulting mixture was stirred for a period of 24 hours. Subsequently, it was introduced to 100 milliliters of methanol to induce precipitation of the polymer.

**3.3: preparation of Poly(3HT-CO-Thiophene)**

Poly(3-hexylthiophene-co-thiophene) were synthesized using varying ratios of 3-hexylthiophene and thiophene, Prepared by addition polymerization method as outlined in **Table 1**.

**Table(1):** show synthesized using varying ratios of 3-hexylthiophene and thiophene.

samples	hexylthiophene	Thiophene
1	50%	50%
2	70%	30%
3	90%	10%

Based on the outcomes of our research, it was determined that the optimal blend consists of 70% 3HT and 30% thiophene.

**3.4: Core shell polymerization of poly (3HT-CO-Th) @ NPs (  $\text{SiO}_2$  , ZnO , Ag )**

In the context of core-shell polymerization, 3-hexylthiophene-Co-thiophene was employed in conjunction with  $\text{SiO}_2$  , ZnO , Ag Nano-particles. To initiate the process, 0.84 grams of the 3-hexylthiophene@thiophene mixture)In different proportions as shown in the table(2) , along with the nano-particles, were introduced into a 50-milliliter  $\text{CHCl}_3$  solution. This solution underwent degassing with  $\text{N}_2$  for approximately 5 minutes while subjected to ultrasound for a half-hour duration[14].

Subsequently, a slurry was formed by adding 1.62 grams of  $\text{FeCl}_3$  to the mixture along with an additional 50 milliliters of  $\text{CHCl}_3$ .

The resulting reactant mixture was stirred for 24 hours. To precipitate the polymer, 100 milliliters of methanol were introduced into the solution.



**4: Results and discussion**

**Table( 2): The table represents a summary of the samples**

samples	Sample summary
P3HT	Poly1
thiophene	Poly2
(70% P3HT-CO-30%PTH )	Co-Poly3
(70% P3HT-CO-30%PTH ) @ (25% ZnO Np)	Co-Poly4
(70% P3HT-CO-30%PTH ) @ (25% SiO <sub>2</sub> Np)	Co-Poly5
(70% P3HT-CO-30%PTH ) @ (25% Ag Np)	Co-Poly6

**4.1: Fourier Transform Infrared (FT-IR) spectrums**

We used the FTIR device from University of Basra, College of Science, Department of Chemistry.

The FTIR analysis of Poly(3HT-CO-Thiophene)@nano SiO<sub>2</sub>, ZnO, and Ag composite material showed fig (1, 2, 3) would likely reveal distinct peaks at characteristic wavenumbers corresponding to various functional groups. For the polymer, peaks might appear at around 3000-2800 cm<sup>-1</sup> for C-H stretching vibrations, 1600-1500 cm<sup>-1</sup> for aromatic C=C stretching vibrations, and potentially in the region of 1000-700 cm<sup>-1</sup> for S-containing functional groups like C-S or S-H bonds from the thiophene units[15].

In the case of SiO<sub>2</sub>, strong peaks can be anticipated at approximately 1100-1000 cm<sup>-1</sup> for Si-O-Si stretching vibrations. Variations or shifts in these peaks when in the composite material would suggest interactions between the polymer and SiO<sub>2</sub>, manifesting as changes in peak positions or intensities[16].

Silver nanoparticles (Ag) might contribute to the spectrum with peaks around 600-400 cm<sup>-1</sup>, potentially indicating Ag-O or Ag-C bonds. Any shifts or changes in these regions compared to the individual components would signify potential bonding or interactions between the polymer and the respective nanoparticles[17]



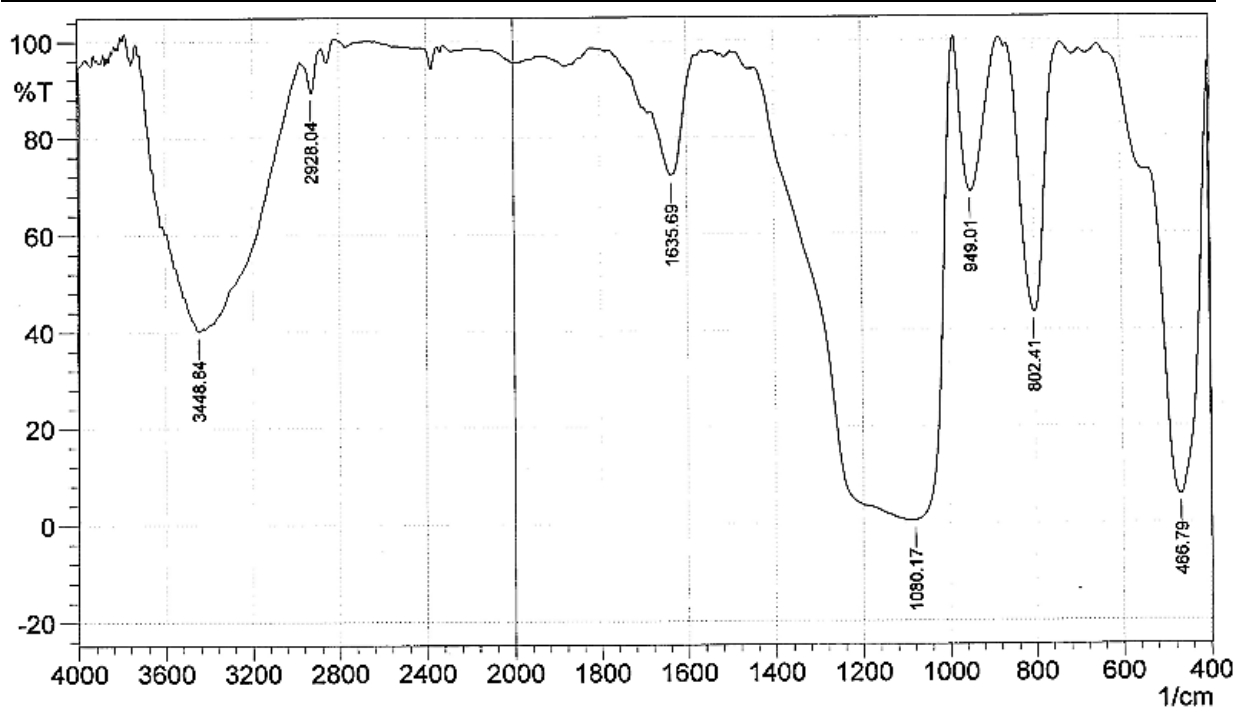


Figure (1) FT-IR Spectroscopy of Co-Poly4

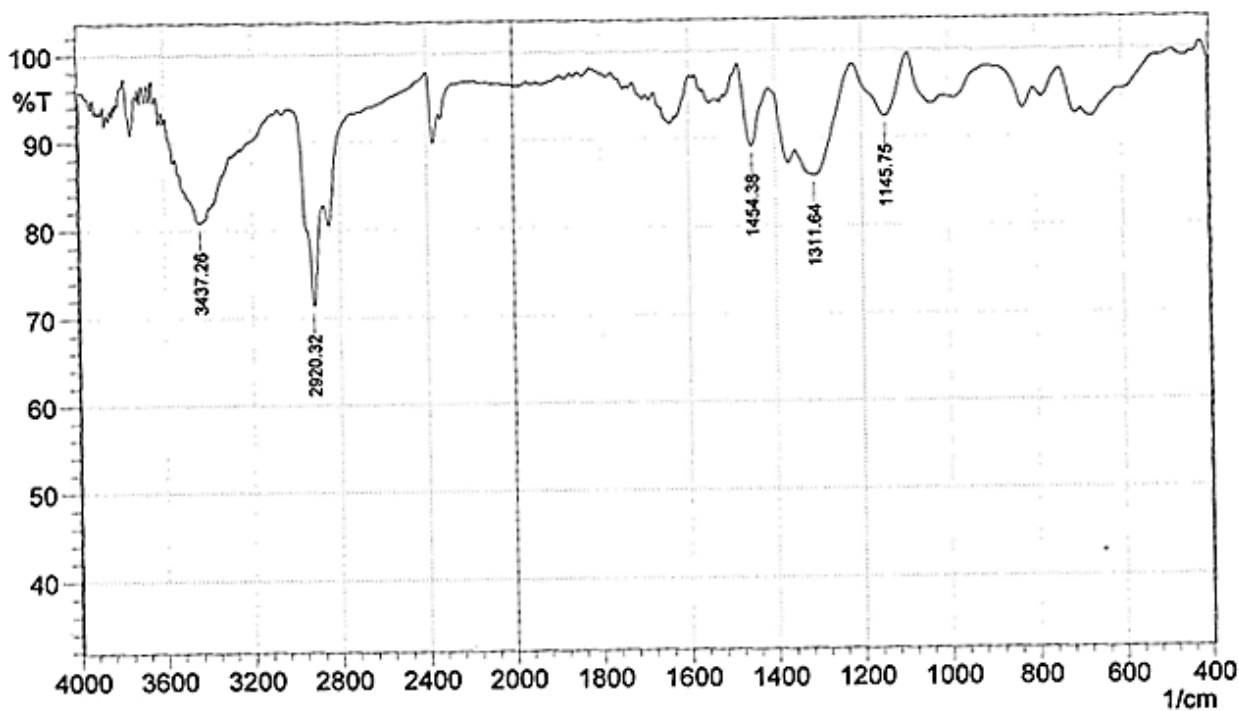


Figure (2) FT-IR Spectroscopy of Co-Poly5



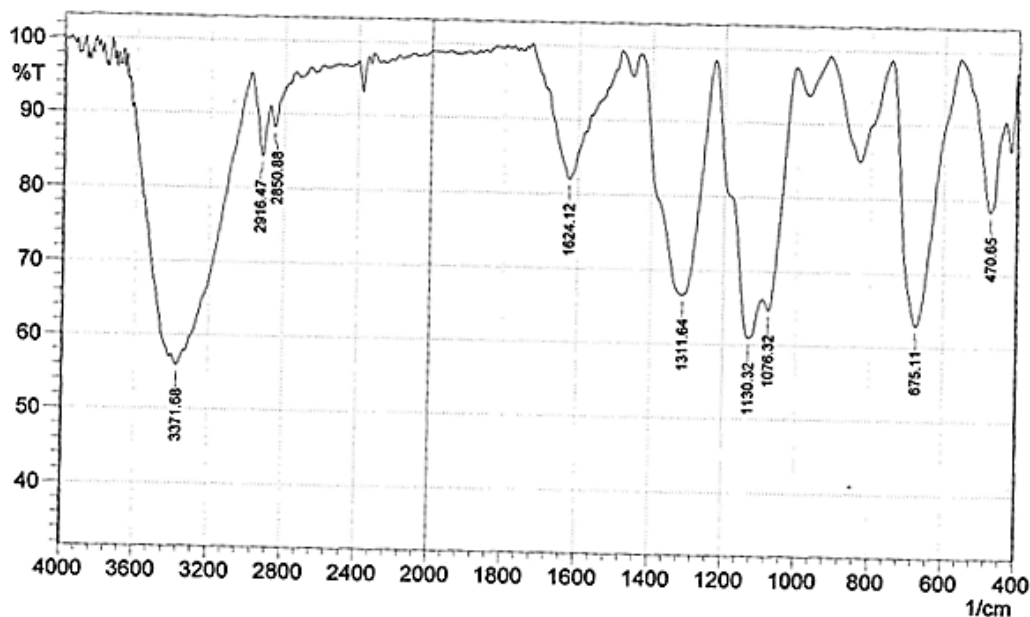


Figure (3) FT-IR Spectroscopy of Co-Poly6

#### 4.2: Scanning Electron Microscopy Analysis of P3HT Films

In Figure( 4 , 5 , 6 ) we present scanning electron microscopy (SEM) images of a heterojunction . These images provide a visual representation of the SEM measurements conducted on the sample. Notably, they reveal the presence of an intermediate layer within the heterojunction. This intermediate layer exhibits the formation of an interpenetrated network throughout the active layer film, resulting in a textured surface with uniformly distributed flake-like grains. Upon closer examination, we conducted detailed analyses that yielded intriguing insights. In one instance, the variable range measured was less than 100 nanometers, specifically between (70% P3HT + 30% thiophene) and (25% ZnO NP), reaching a minimum value of 70 nanometers. However, in cases of complete agglomeration, the thickness extended to 120.45 nanometers (In shape 6).

As a significant outcome of our investigations, it was determined that the polymeric film formed on the nanoparticles in the samples ranged from 5 nanometers to 19 nanometers of (Poly ( 70% 3HT +30% Th)@ (25% Ag Nano particles) . This range of polymer layer thickness is crucial, as it classifies the layer as transparent, with the ability to transmit a substantial amount of light.

In summary, our SEM analysis not only provides a visual glimpse into the heterojunction structure but also offers valuable data on the thickness and characteristics of the polymer layer, which is instrumental in its light-transmitting properties.



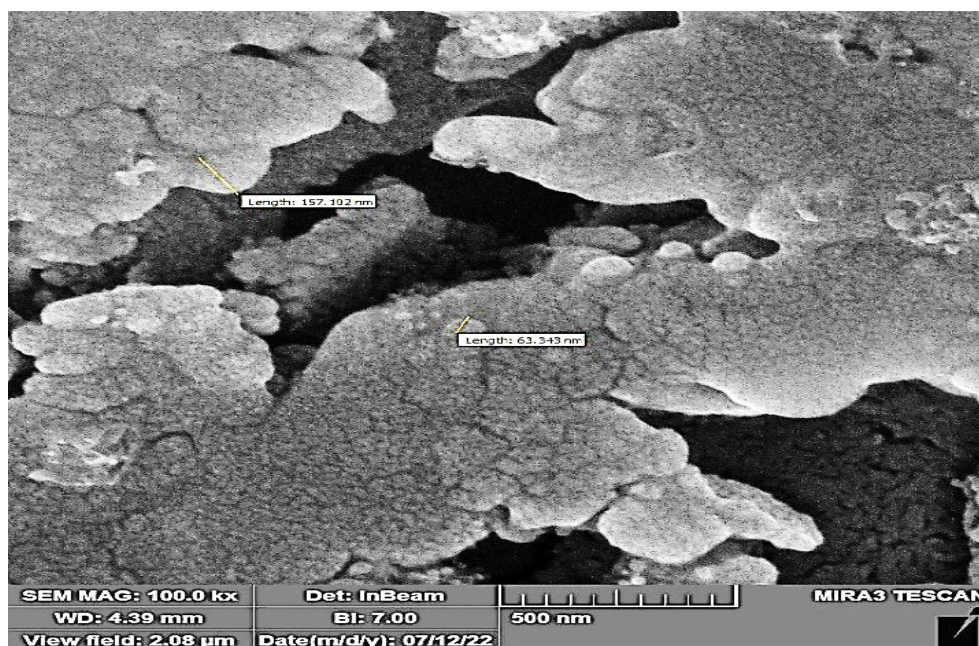


Figure (4) Scanning Electron Microscopy of Co-Poly4

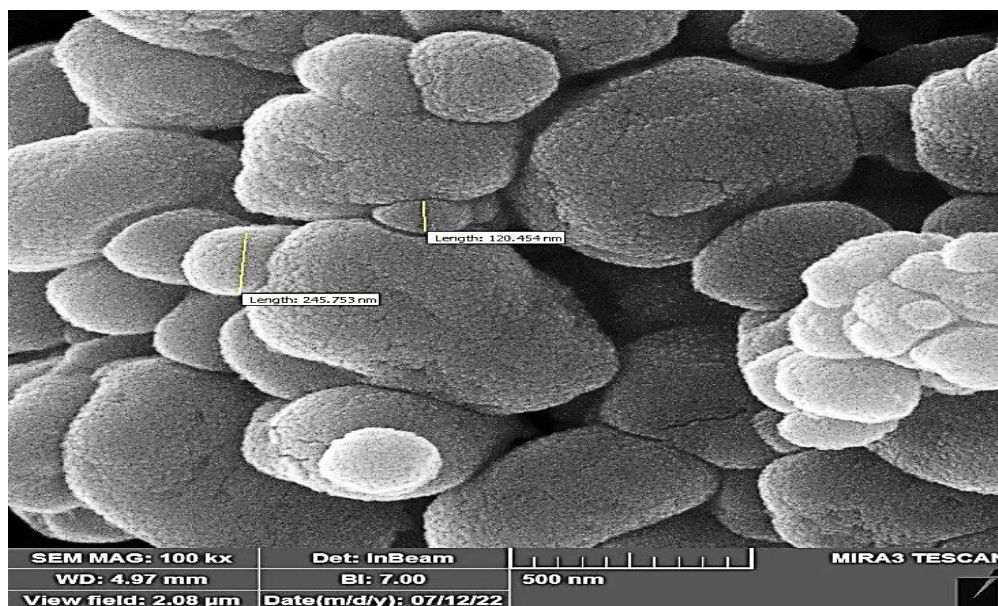


Figure ( 5 ) Scanning Electron Microscopy of Co-Poly5



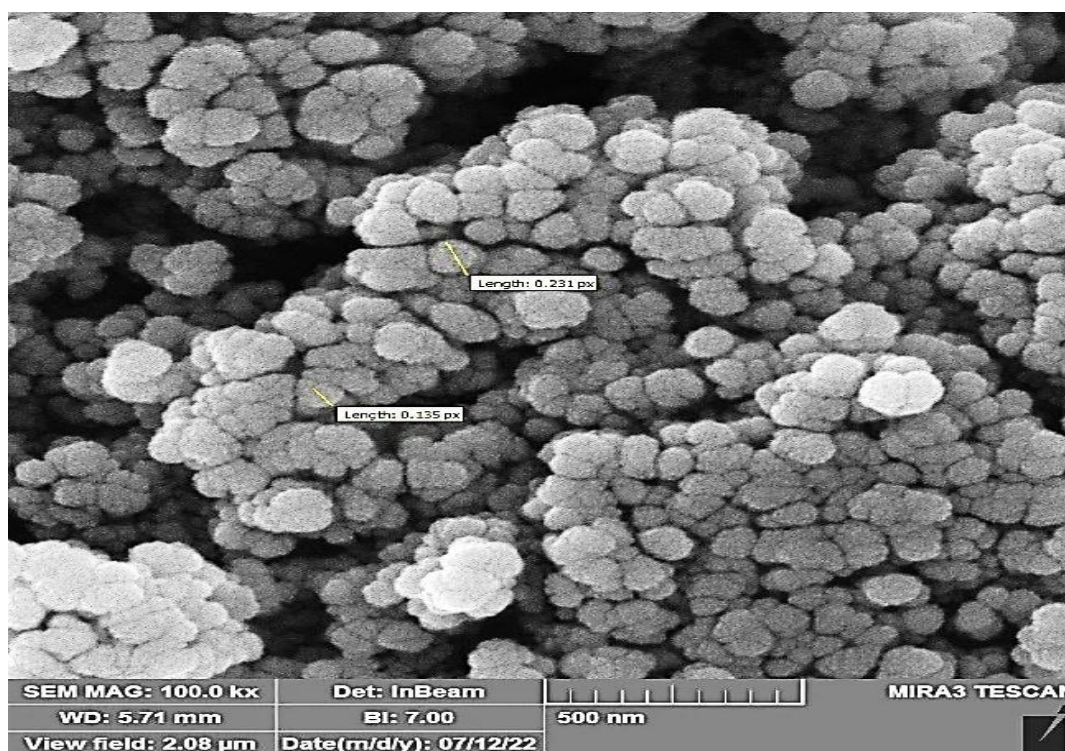


Figure (6) Scanning Electron Microscopy of Co-Poly6

#### 4.3: Atomic Force Microscopy (AFM) Analysis

We used the Atomic Force Microscopy device from University of Tehran, Iran (Newport Multimode™ Model 401).

To investigate the surface properties of Nano polymer membranes, these polymers were meticulously deposited onto silicon substrates. During the measurement process, the tip mode of an atomic force microscope (AFM) was employed.

The accompanying figures (from 7 to 12) show cases a sequence of images captured using AFM, each depicting a different dimension of the polymeric surfaces (10 nm ). It's important to note that these measurements were conducted under standard environmental conditions.

The images reveal intriguing details. Notably, areas with a smaller cross-section exhibit more pronounced grain sizes. Furthermore, we observe the consistent formation of atomic structures and similar shape features across these polymeric surfaces. Additionally, clusters of atoms and molecules are discernible. These clusters may arise from variations in the binding energy of chemical bonds within the polymer structure.

Furthermore, the AFM imaging allows us to gain insights into the three-dimensional structure of the polymeric membrane, providing a thorough examination of its thickness, which measures approximately between 155 to 5.35 nanometers, It was compared with some published research[18].



In terms of surface roughness, the polymer film exhibits values ranging from 73.9 nanometers to 5.19 nanometers. It was compared with some published research[19 ,20 ,21].

AFM analysis unveils valuable information about the surface properties of Nano polymer membranes, including the distribution of grain sizes, the presence of atomic clusters, and the surface roughness , all of which contribute to a comprehensive understanding of the material's characteristics and potential applications.

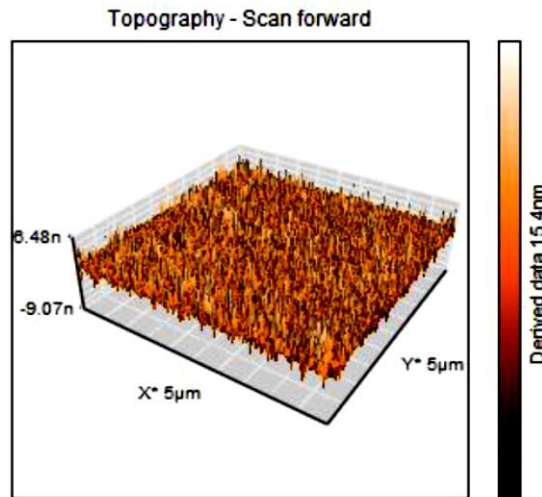


Figure (7 ) Atomic Force Microscopy of Poly1

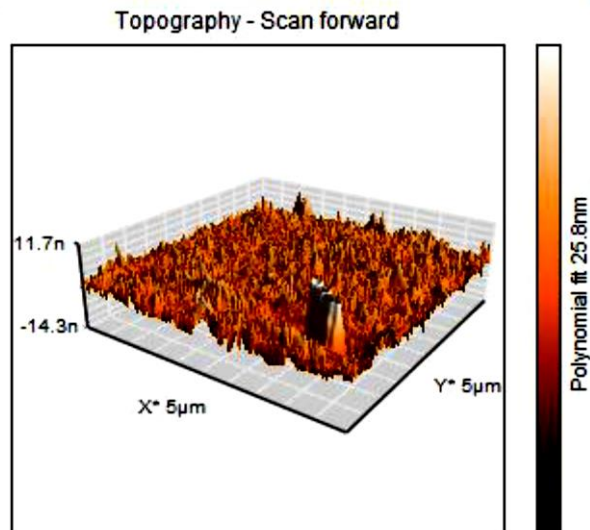


Figure (8) Atomic Force Microscopy of Poly2



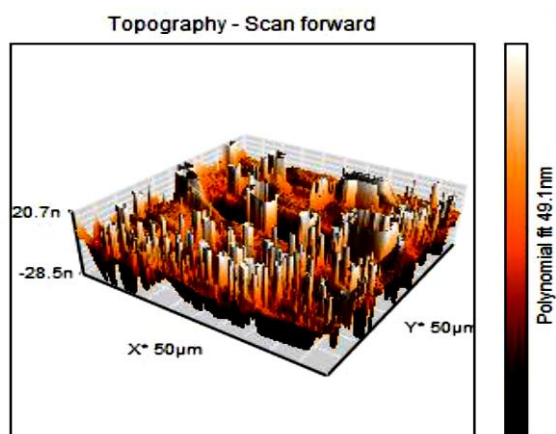


Figure (9 ) Atomic Force Microscopy of Co-Poly3

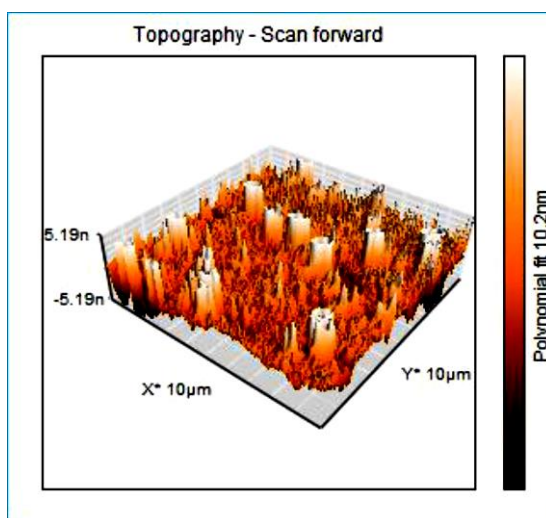


Figure (10 ) Atomic Force Microscopy of P Co-Poly4

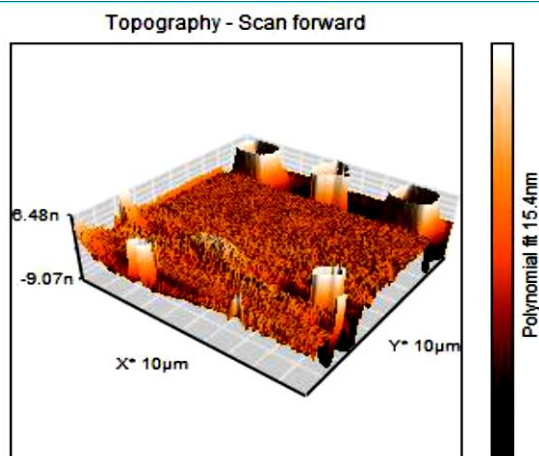


Figure (11 ) Atomic Force Microscopy of Co-Poly5



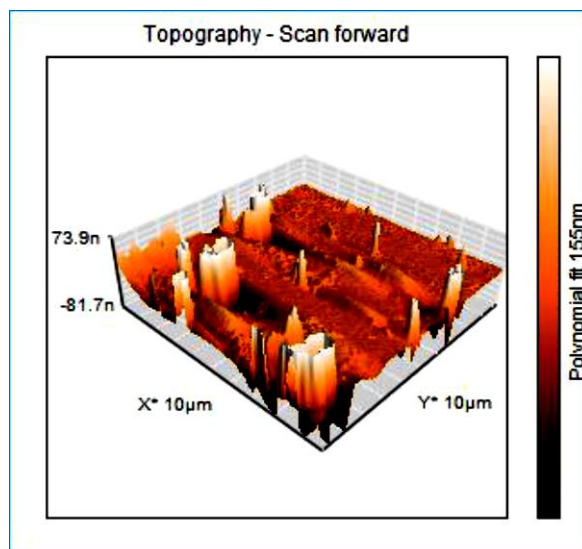


Figure (12 ) Atomic Force Microscopy of Co-Poly6

#### 4.4: X-Ray Diffraction (XRD) Analysis

We used X-Ray Diffraction device from University of Tehran, Iran .

The study utilized X-ray diffraction (XRD) to examine material structures, fig (13 , 14 , and 15) for revealing several key insights.

Polymers, due to their low X-ray absorption, allow minimal interference, yet even highly crystalline ones contain amorphous regions owing to inherent structural irregularities.

Achieving a completely monocrystalline polymer structure is challenging due to these complexities. Broad XRD peaks indicate structural defects within polymers, while higher polymer crystallinity necessitates high viscosity and low permeability for a more ordered molecular arrangement. Specific XRD patterns of P3HT and Thiophene highlighted indicating crystallinity in P3HT and an amorphous structure in Thiophene. Quantitative peak data provided crucial insights into material crystalline properties, enabling the distinction between crystalline and amorphous phases and offering valuable information on material structural behaviors.

From the results of the X-ray analysis shown in the tables, the crystal lattice parameter was obtained, and these results are identical to the sources [22 , 23 , 24 , 25 , 26 ].

X-ray diffraction pattern of the formed nanoparticles is shown in Figure (13 , 14 , and 15). A number of Bragg reflection peaks were observed at  $2\theta$  values of  $(11.79693^\circ)$  ,  $(22.0942^\circ)$  ,  $(26.09385^\circ)$  ,  $(27.94658^\circ)$  ,  $(32.3605^\circ)$  ,  $(46.5021^\circ)$  ,  $(55.0399^\circ)$  ,  $(57.66864^\circ)$  ,  $(67.76884^\circ)$  ,  $(74.66813^\circ)$  and  $(76.91441^\circ)$  which are indexed  $(200)$ ,  $(110)$ ,  $(111)$ ,  $(210)$ ,  $(231)$ ,  $(142)$ ,  $(241)$ ,  $(200)$  ,  $(004)$  and  $(311)$ .



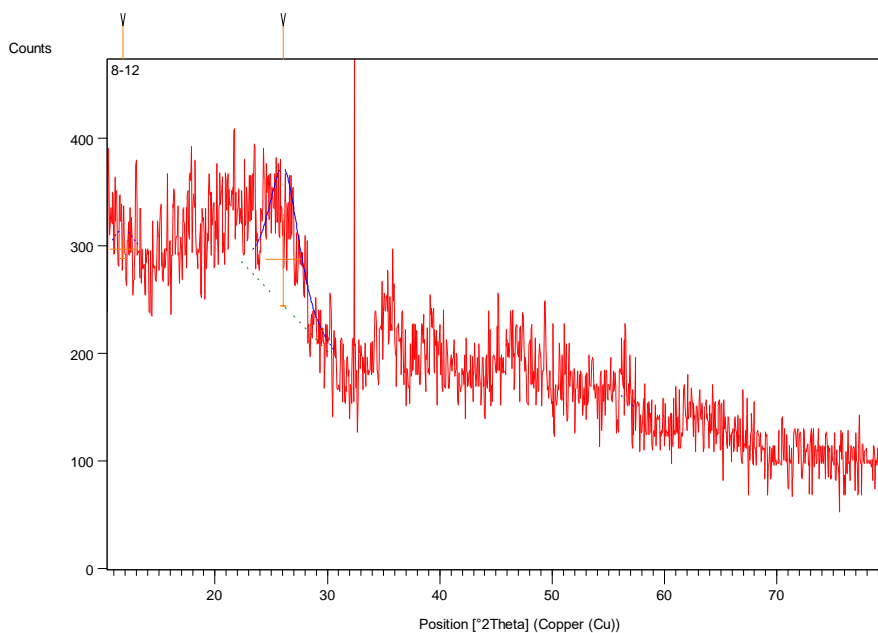


Figure (13) X-Ray Diffraction of Co-Poly4

Table 3: X-ray diffraction data for Co-Poly4

Pos. [°2Th.]	Height [cts]	FWHM [°2Th.]	d-spacing [Å]	Rel. Int. [%]	Tip Width
11.79693	17.80933	2.3616	7.50187	20.76	2.8339
26.09385	85.77493	3.1488	3.41502	100	3.7786

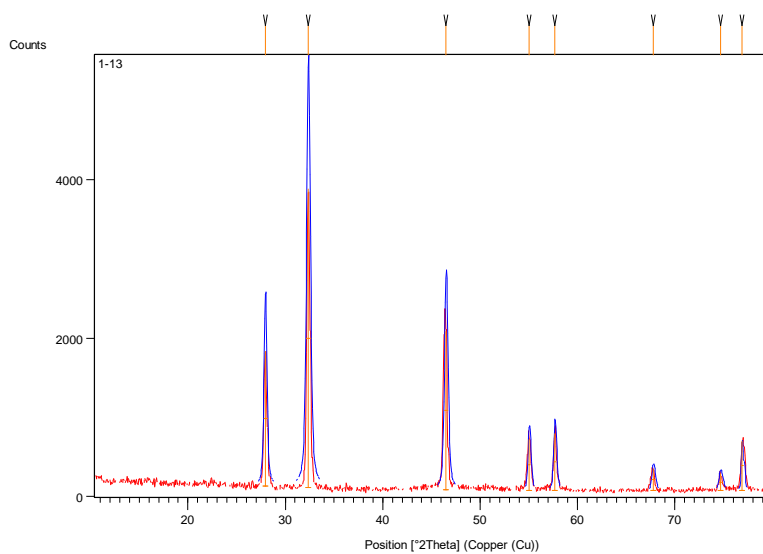
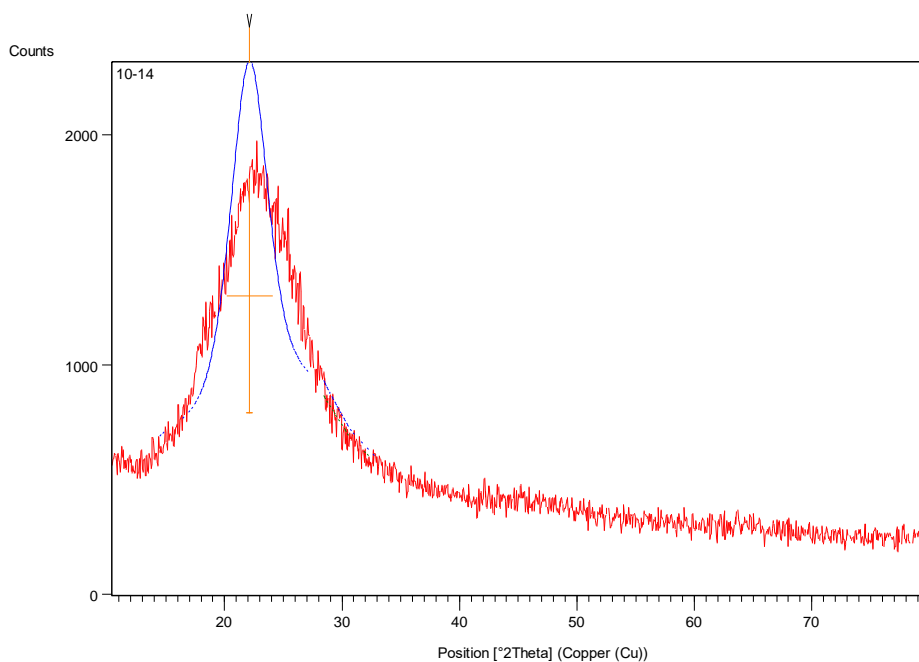


Figure (14): X-Ray Diffraction of Co-Poly5



**Table 4:** X-ray diffraction data for **Co-Poly5**

Pos. [ $^{\circ}2\theta$ .]	Height [cts]	FWHM Left [ $^{\circ}2\theta$ .]	d-spacing [Å]	Rel. Int. [%]	Tip Width
27.94658	1711.22	0.3444	3.19269	45.31	0.4133
32.3605	3776.989	0.4428	2.76659	100	0.5314
46.5021	2003.696	0.3936	1.95292	53.05	0.4723
55.0399	647.4111	0.2952	1.66849	17.14	0.3542
57.66864	720.3184	0.2952	1.59853	19.07	0.3542
67.76884	277.5717	0.3444	1.3828	7.35	0.4133
74.66813	213.3581	0.3936	1.27121	5.65	0.4723
76.91441	637.7366	0.1968	1.23959	16.88	0.2362



**Figure (15):** X-Ray Diffraction of **Co-Poly6**

**Table 5** X-ray diffraction data for **Co-Poly6**

Pos. [ $^{\circ}2\theta$ .]	Height [cts]	FWHM Left [ $^{\circ}2\theta$ .]	d-spacing [Å]	Rel. Int. [%]	Tip Width
22.0942	1021.857	3.84	4.02002	100	4.608



#### 4.5: Optical Properties

We used UV device in University of Basra, College of Education for Pure Sciences, Department of Physics (shimadzu corporation Japan , UV -1800 240V ).

Copolymer films deposited onto glass substrate after annealing at 70 °C for 30 min in the wavelength between 200 - 800 nm.

the main absorption wavelength region of samples **Co-Poly4** , **Co-Poly5** , **Co-Poly6** is around  $\lambda \sim 500$  nm . The UV- absorption spectra of the all films were plotted in Figure (16) featured absorption bands around  $\lambda \sim 490, 500$  and 510 nm , respectively.

The main peak at  $\sim 490$  nm is attributed to the  $\pi-\pi^*$  transition in crystalline  $\pi-\pi$  stacking structure of polymer P3HT chains (conjugated polymer)[27].

The variation of absorbance with wavelength for samples **Co-Poly4** , **Co-Poly5** , **Co-Poly6** are shown in figure ( 16) . The figure show peak appears at 500nm for **Co-Poly4** .

From drawing the relationship between absorption coefficient and photon energy of **Co-Poly4** , **Co-Poly5** , **Co-Poly6** .

The value of absorption coefficient plays an important role in the limitation of the type of transition. From the above figures the value of the ( $\alpha$ )was greater than ( $10^4 \text{ cm}^{-1}$ ) indicating that the transition was direct electron transmission.

The figs. ( from 17 to 22) provided illustrates the relationship between  $(h\nu)$  versus  $(h\nu\alpha)^2$  and the photon energy of the samples.

The energy gap was determined by identifying the intersection point of the linear relationship with  $h\nu$  yielding values of approximately( 2.78 eV for thiophene and 2.3 eV for **Poly1** While for samples **Co-Poly4** , **Co-Poly5** , **Co-Poly6** (1.78 eV , 1.82 eV , 1.75 eV respectively) , While copolymers **Co-Poly3** without nanoparticles had greater The energy gap (1.88) .

**Table 7:** presents the energy gap values for the various samples. Notably, a discernible trend emerges from the figures: the energy gap diminishes as nanoparticles are introduced, decreasing from(2.3 eV) to (1.75 eV). This signifies a reduction in the energy gap by 0.25 eV following doping.

The decrease in the energy gap can be elucidated by the heightened concentration of nanoparticles. As doping levels increase, there is an augmentation in the number of polar on states introduced within the energy gap, ultimately leading to its contraction[28].

Moreover, the increase in the absorption coefficient observed with increasing nanoparticle concentration can be attributed to the absorption of additional photons by the newly generated energy levels within the gap. These levels multiply in number as doping levels rise, contributing to the augmented absorption coefficients[29].

The analysis of optical properties, specifically the energy gap and absorption coefficients, provides valuable insights into the impact of nanoparticle doping on the material's electronic structure, shedding light on its potential applications in optoelectronic devices[30].

The refractive index dispersion can be analyzed by the single-oscillator model [31].

$$n^2 + 1 = \frac{E_d + E_o}{E_o^2 - (h\nu)^2} \dots \dots \dots (5)$$



Where n is the refractive index, h is Planck's constant, v is the frequency, ( h v ) is the photon energy, E<sub>o</sub> is the average excitation energy for electronic transitions, and E<sub>d</sub> is the dispersion energy which is a measure of the strength of interband optical transitions. From the drawing between (  $\frac{1}{n^2-1}$  ) versus (hv)<sup>2</sup> Fig( from 23 to 28 ).The oscillator parameters E<sub>o</sub> and E<sub>d</sub> values were determined from the slope (E<sub>o</sub> E<sub>d</sub>)<sup>-1</sup> and the intercept (E<sub>o</sub>/E<sub>d</sub>) on the vertical axis respectively.

From there it was determined the values of the oscillator parameters (E<sub>o</sub>, and E<sub>d</sub>)

The oscillator energy, E<sub>o</sub> is related to the optical band gap.

tabulated in table (7). It is known that inter-material boundaries contain structural defects and impurities. These factors have a strong influence on the absorption processes [32].

The long wavelength refractive index (n<sub>∞</sub>) and average oscillator wave length (λ<sub>o</sub>) and oscillator length strength S<sub>o</sub> can be estimated by the single oscillator model givenby [33].

$$\frac{n_{\infty}^2 - 1}{n^2 - 1} = 1 - \frac{\lambda_o^2}{\lambda^2} \quad \dots (6)$$

n<sub>∞</sub> Value was obtained from the linear parts of (  $\frac{1}{n^2-1}$  ) versus. (  $\frac{1}{\lambda^2}$  ) Fig.( from 29 to 34 ) from the curve plotted are given in table (7). Eq. (6) become:-

$$n^2 - 1 = \frac{s_o \lambda^2}{1 - \frac{\lambda_o^2}{\lambda^2}} \quad \dots \dots \dots (7)$$

where S<sub>o</sub> = (n<sub>∞</sub> -1)/λ<sup>2</sup> is the average oscillator parameter which is the strength of the individual dipole oscillator. The S<sub>o</sub> value was estimated using Eq. above and are given in table (7).

The M-1 and M-2 moments of the optical spectra are expressed as [34].

$$E_o^2 = \frac{M_{-1}}{M_{-3}}, E_d^2 = \frac{M_3}{M_{-1}} \quad \dots \dots \dots (8)$$

The M-1, M-3 moments were estimated using the above equation and are given in table (7). The M-1, and M-2 moments changed due to the formation coordination of complex. The third order nonlinear susceptibility (χ<sub>3</sub>) has been calculated from the following equation(8) and tabulated in table (7).

$$X^3 = A \left[ \left( \frac{E_o E_d}{4\pi(E_o^2 - (hv)^2)} \right)^4 \right] = \frac{A}{(4\pi)^4 (n^2 - 1)^4} \quad \dots \dots \dots (9)$$

The provided table encapsulates essential optical properties of diverse materials and compositions at distinct wavelengths and energy levels. Each entry delineates parameters crucial in understanding the materials' response to light, encompassing nonlinear optical behavior ( Third-order visual effect X<sup>3</sup> , The Average Oscillator S<sub>o</sub> ) , energy-related



characteristics (Moments Of The Optical Spectra For Liquid Crystal M-3 , Moments Of The Optical Spectra For Liquid Crystal M-1, and key optical traits (refractive index, energy dissipation, band gap energy). For instance, P3HT showcases moderate values across parameters, indicating its potential in specific electronic applications with a band gap energy ( $E_g$ ) of 2.3 eV. Conversely, Polythiophene demonstrates differing optical traits, notably with an  $E_g$  of 2.78 eV. Furthermore, the compositions blending P3HT with varying nanoparticles ( $\text{SiO}_2$  NP, ZnO NP, Ag NP) exhibit distinctive properties, showcasing sensitivity to compositional changes. These findings suggest potential applications in optoelectronics and photonics, implying materials with specific band gap energies may suit distinct uses like solar cells or light-emitting devices. However, further analysis and experimentation are warranted to unravel the full implications and applications of these materials based on their intricate optical properties[35].

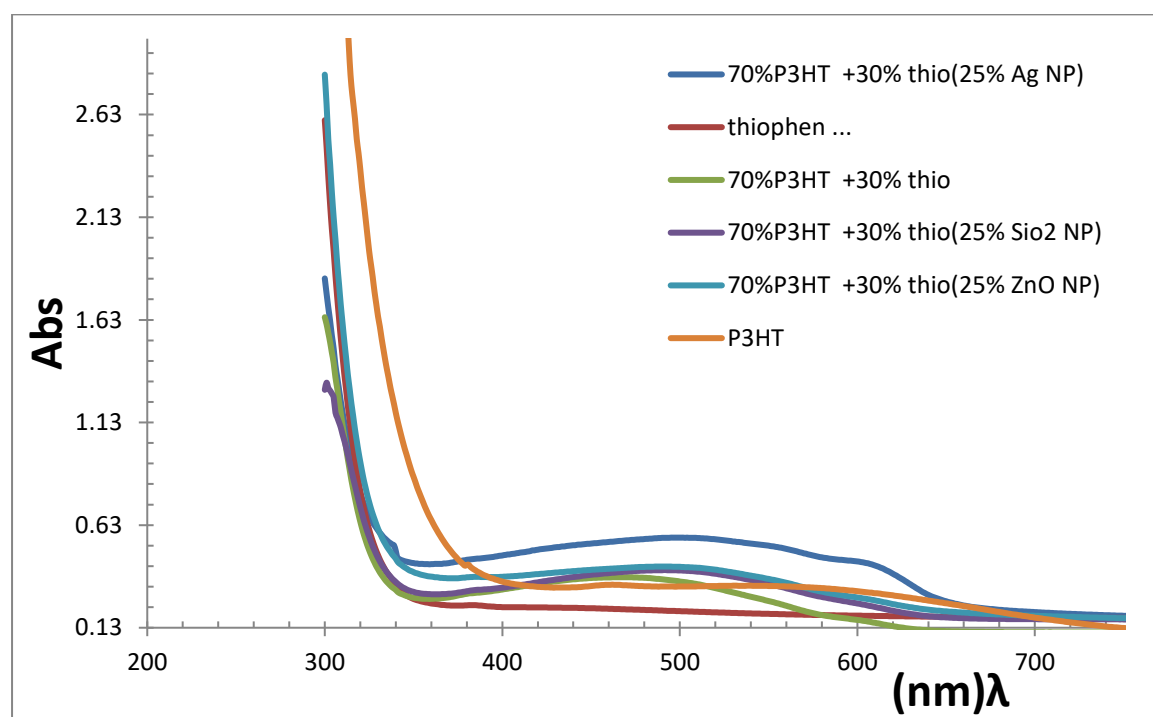


Figure (16) absorption of Poly1 , Poly2 , Co-Poly3 , Co-Poly4 , Co-Poly5 , Co-Poly6



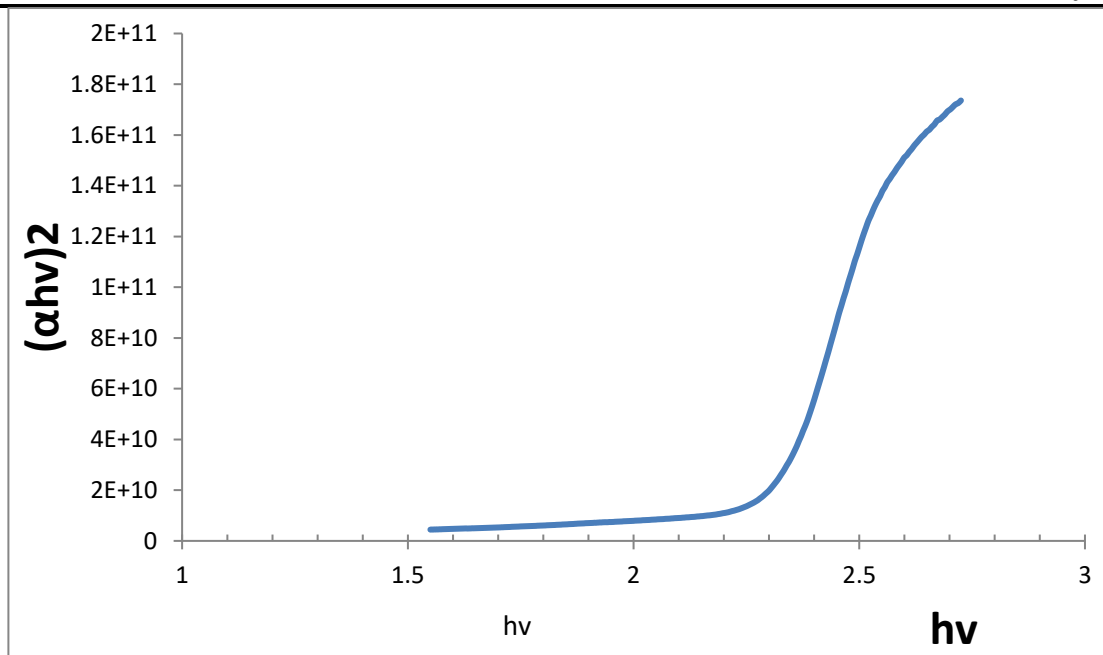


Figure (17) Band gab Energy of Poly1

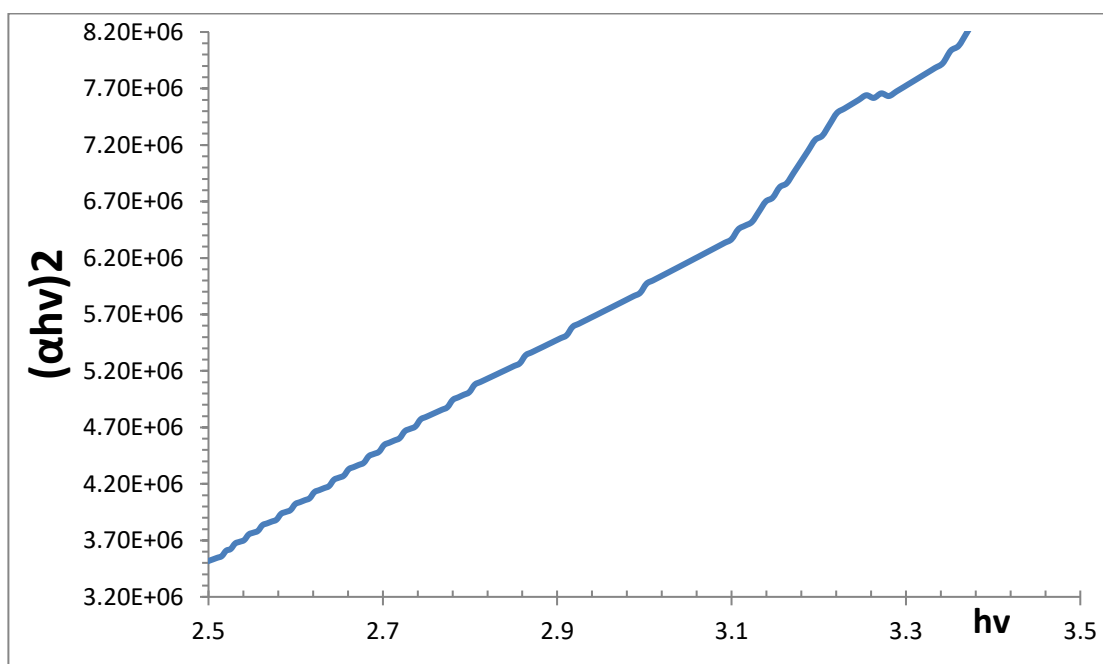


Figure (18) Band gab Energy of Poly2



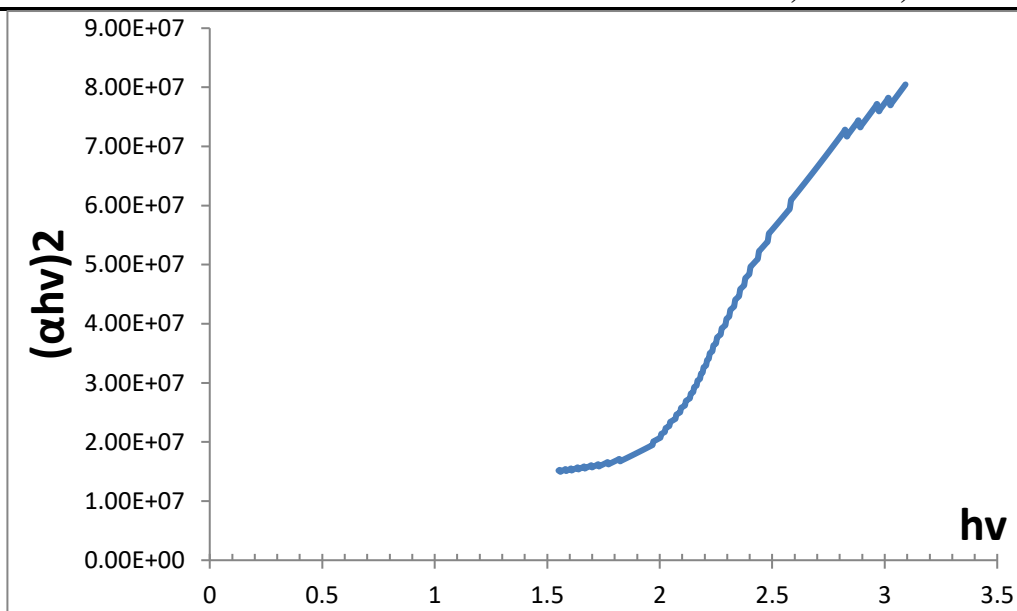


Figure (19) Band gab Energy of Co-Poly3

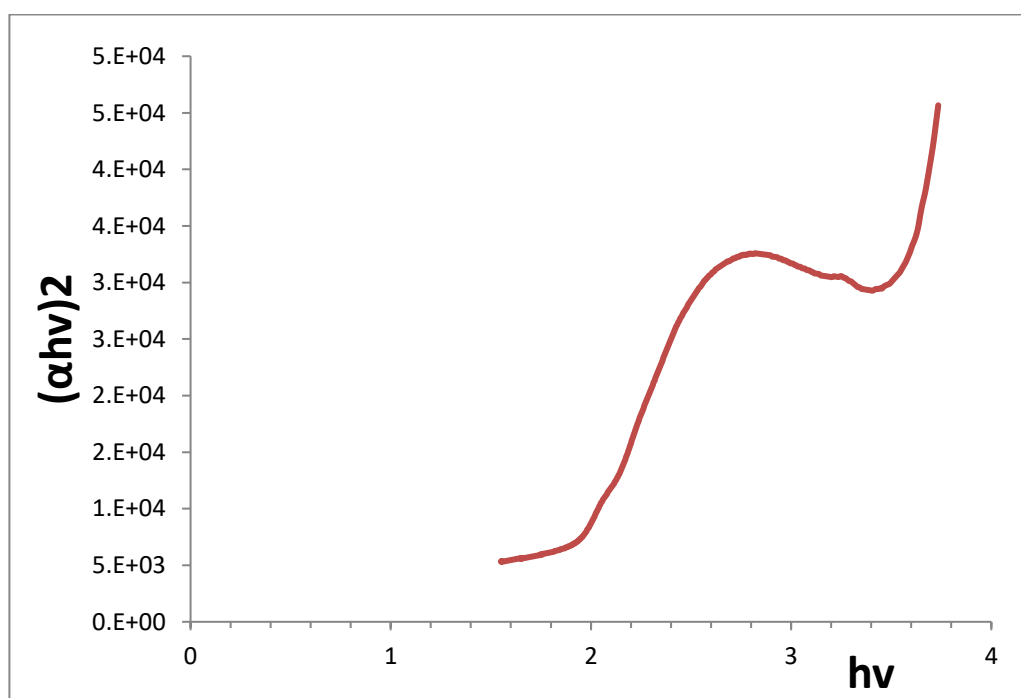


Figure (20) Band gab Energy of Co-Poly4



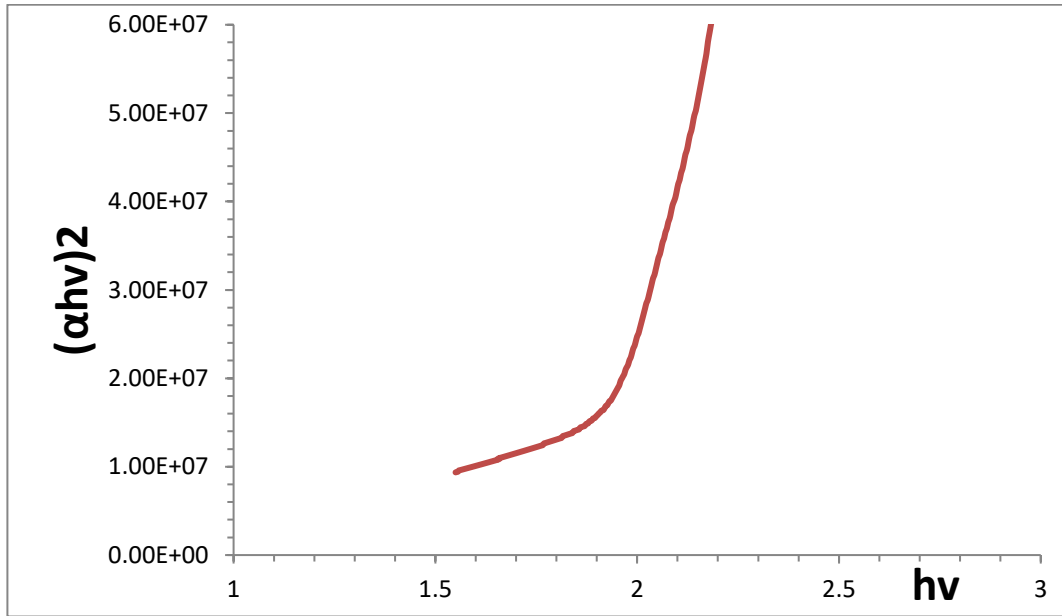


Figure (21) Band gab Energy of Co-Poly5

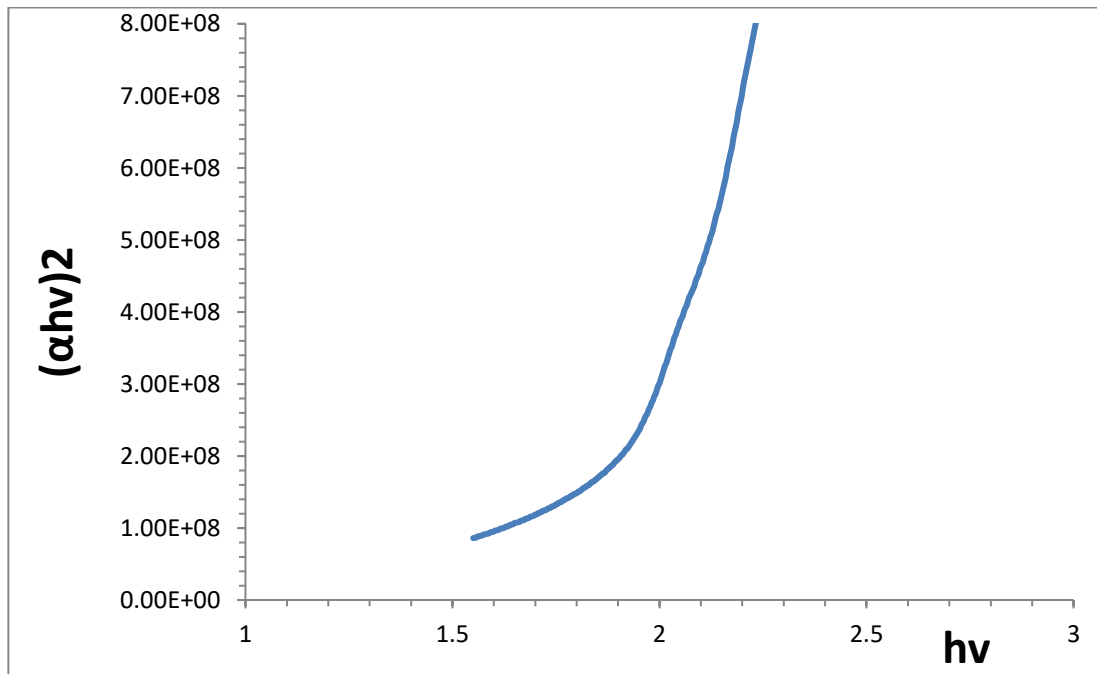


Figure (22) Band gab Energy of Co-Poly6



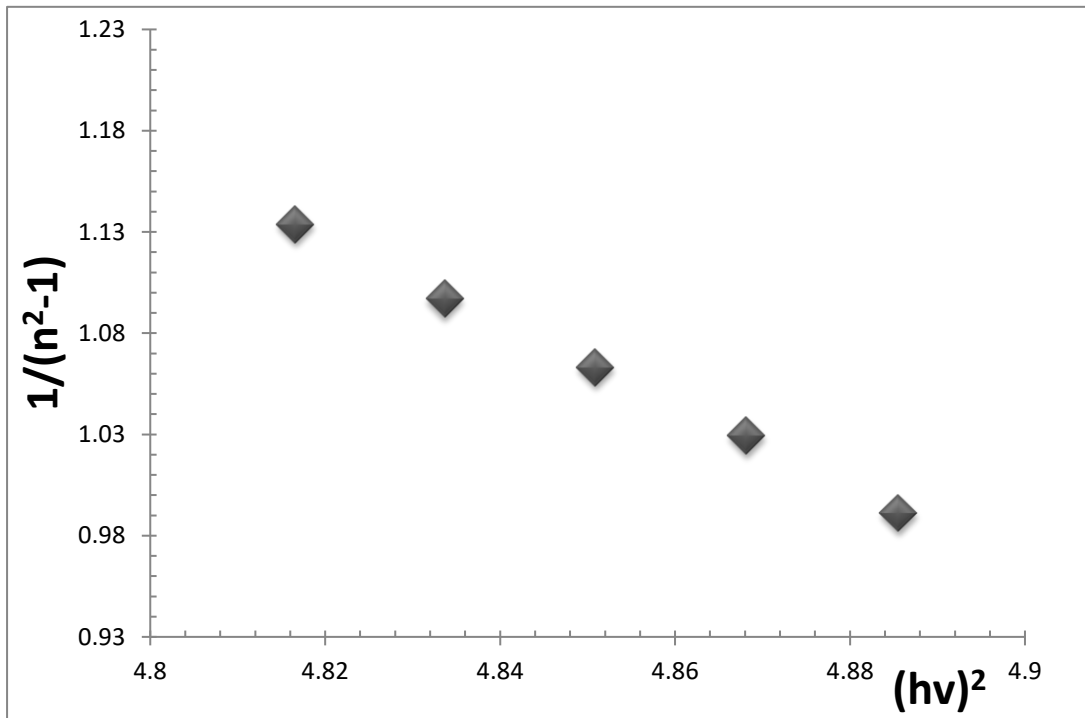


Figure (23) relationship between  $(\frac{1}{n^2-1})$  versus  $(hv)^2$  of Poly1 .

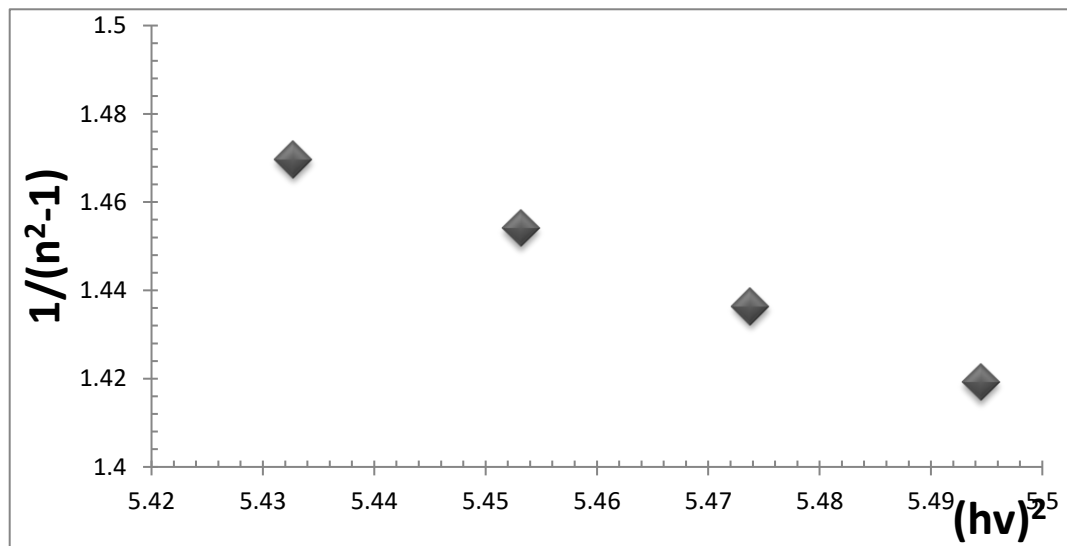


Figure (24) relationship between  $(\frac{1}{n^2-1})$  versus  $(hv)^2$  of Poly2 .



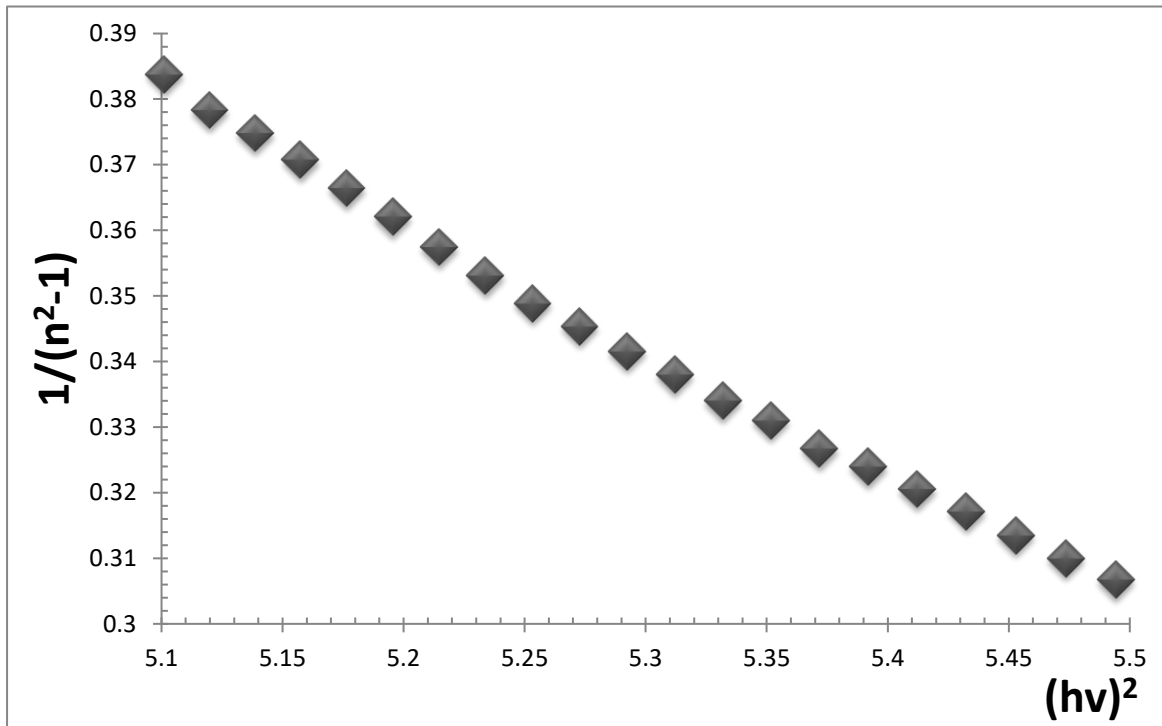


Figure (25) relationship between  $(\frac{1}{n^2-1})$  versus  $(hv)^2$  of Co-Poly3.

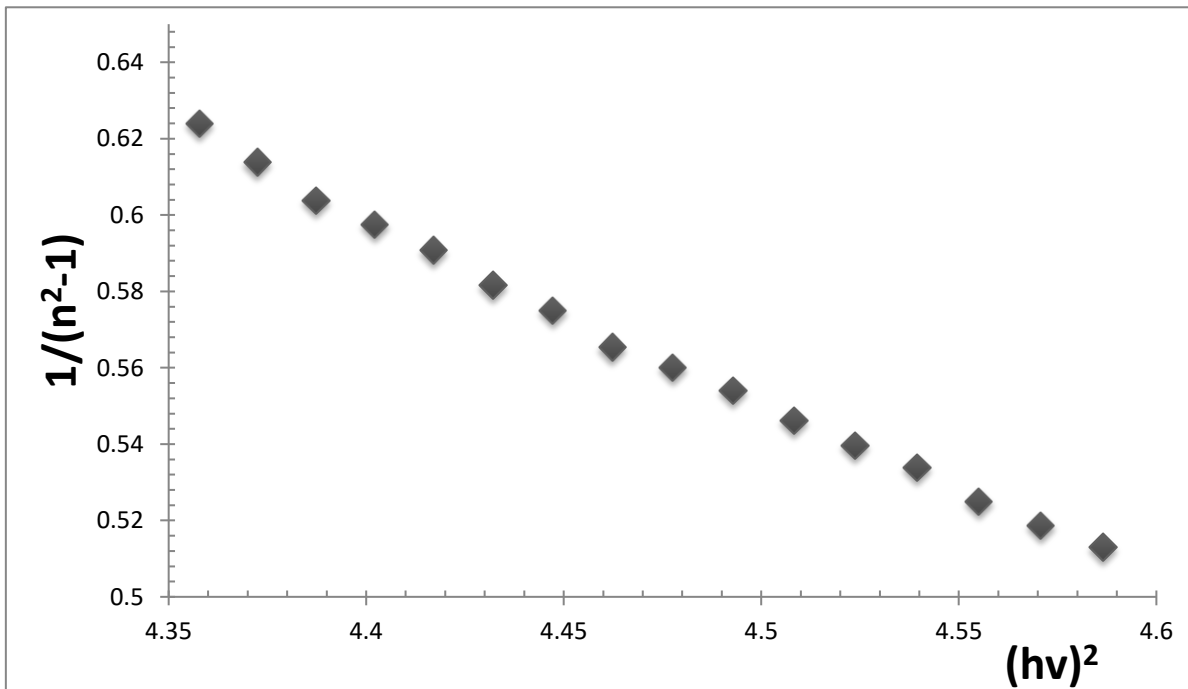


Figure (26) relationship between  $(\frac{1}{n^2-1})$  versus  $(hv)^2$  of Co-Poly4.



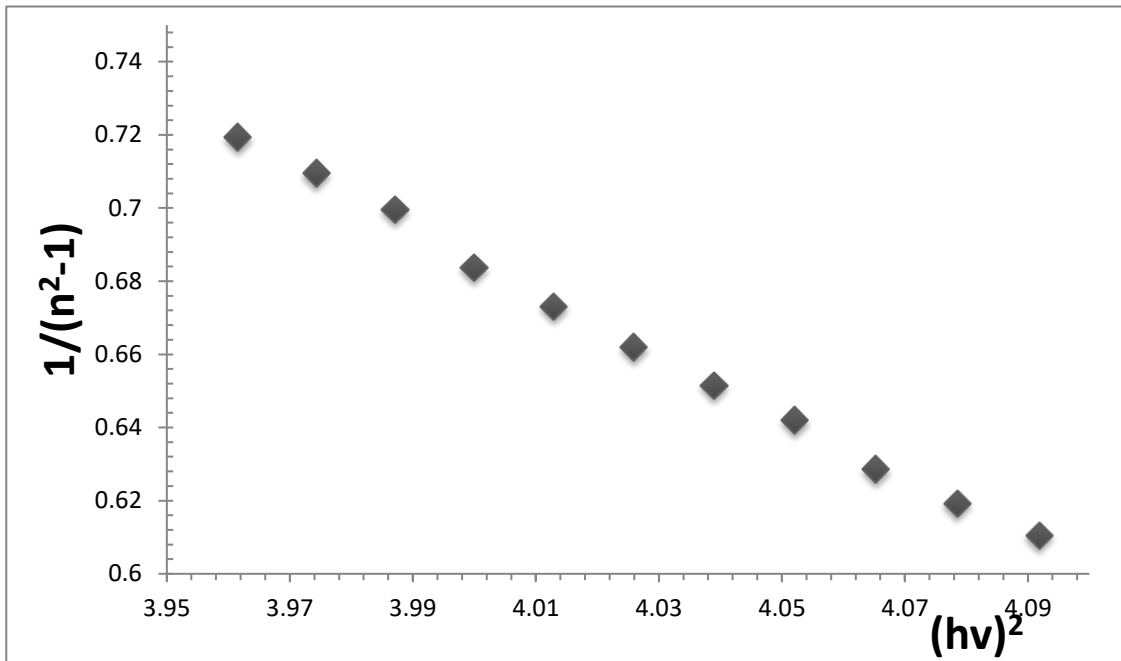


Figure (27) relationship between  $(\frac{1}{n^2-1})$  versus  $(hv)^2$  of Co-Poly5.

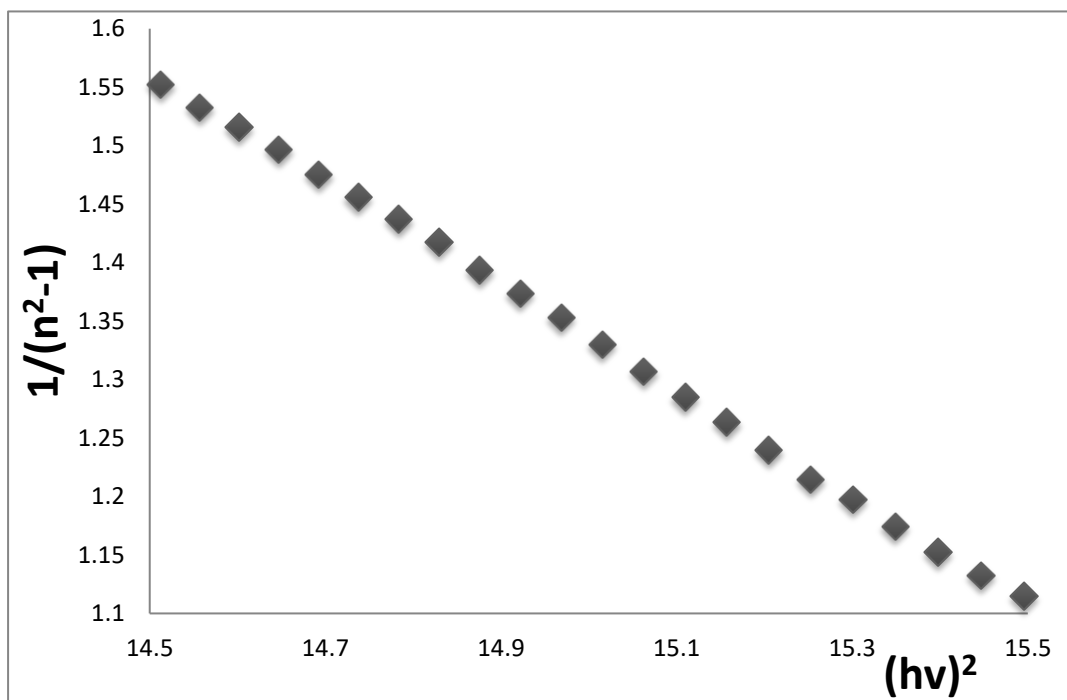


Figure (28) relationship between  $(\frac{1}{n^2-1})$  versus  $(hv)^2$  of Co-Poly6.



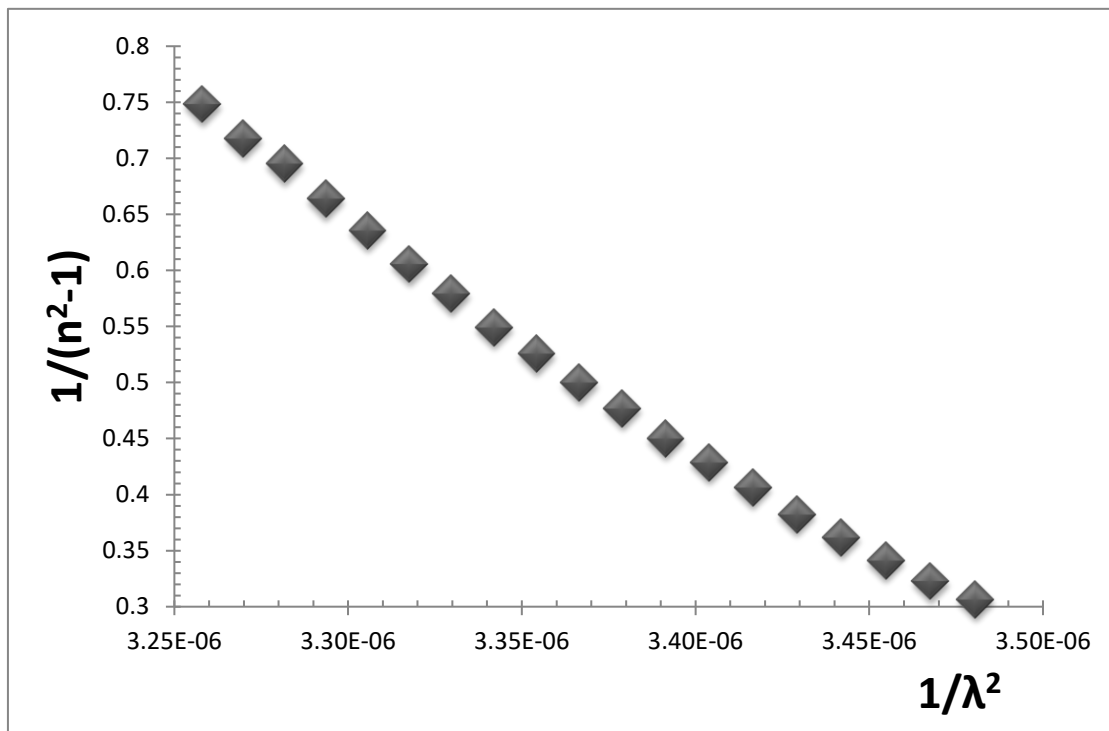


Figure (29) relationship between  $(\frac{1}{n^2-1})$  versus  $(\frac{1}{\lambda^2})$  of Poly1 .

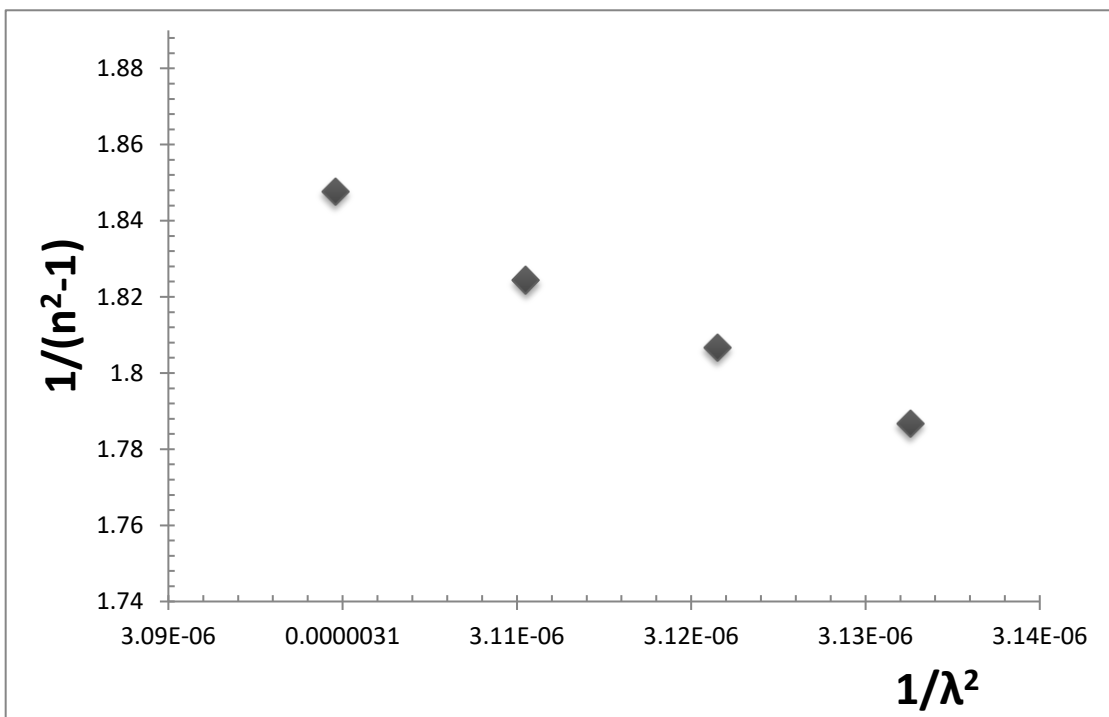


Figure (30) relationship between  $(\frac{1}{n^2-1})$  versus  $(\frac{1}{\lambda^2})$  of Poly2 .



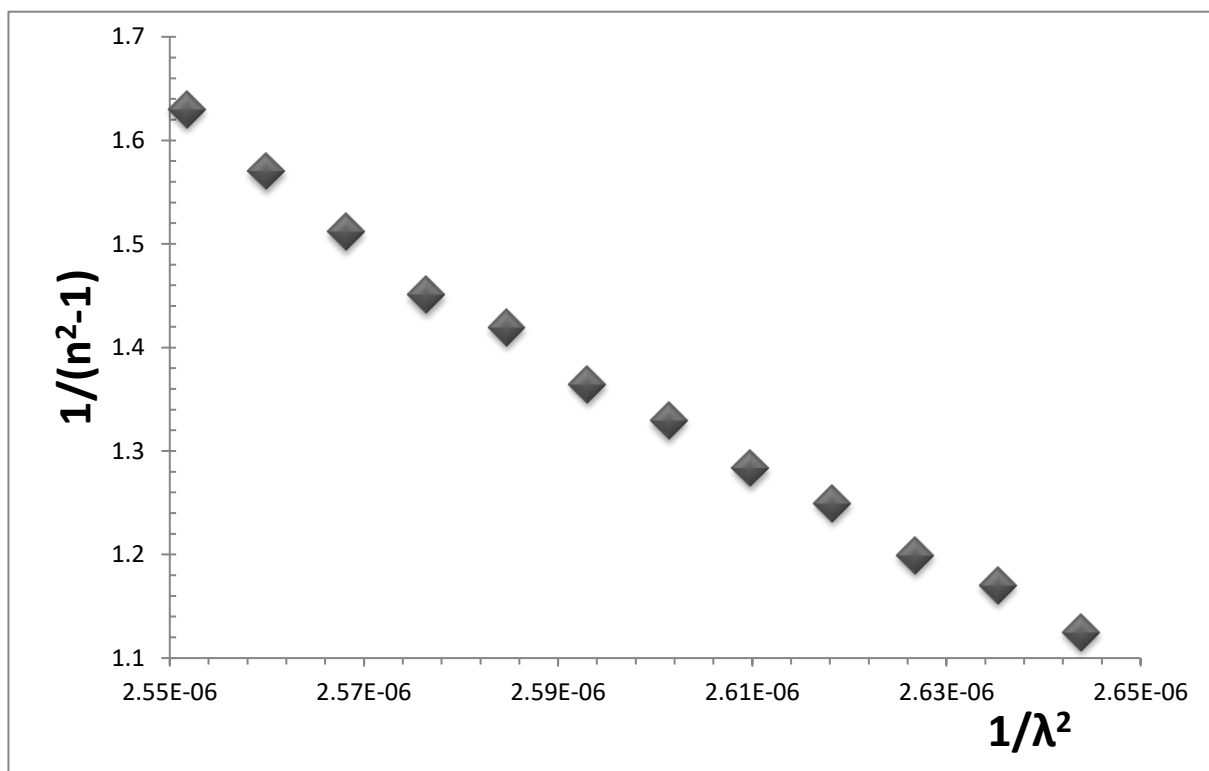


Figure (31) relationship between  $(\frac{1}{n^2-1})$  versus  $(\frac{1}{\lambda^2})$  of Co-Poly3.

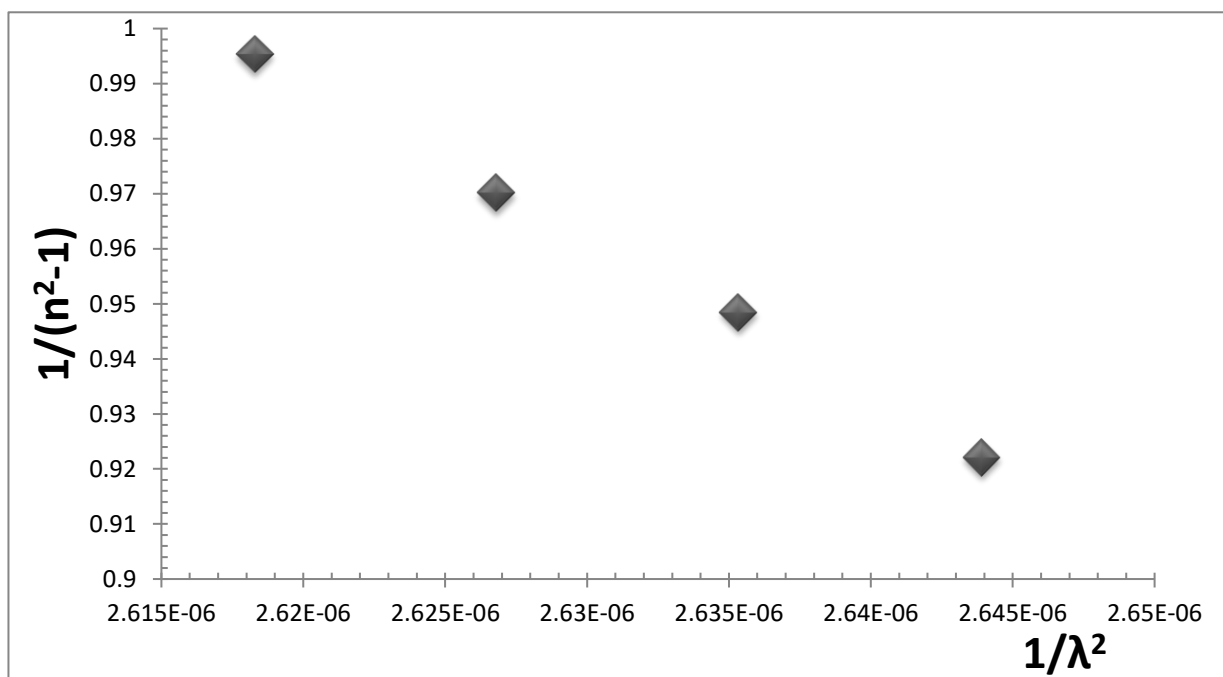


Figure (32) relationship between  $(\frac{1}{n^2-1})$  versus  $(\frac{1}{\lambda^2})$  of Co-Poly4.



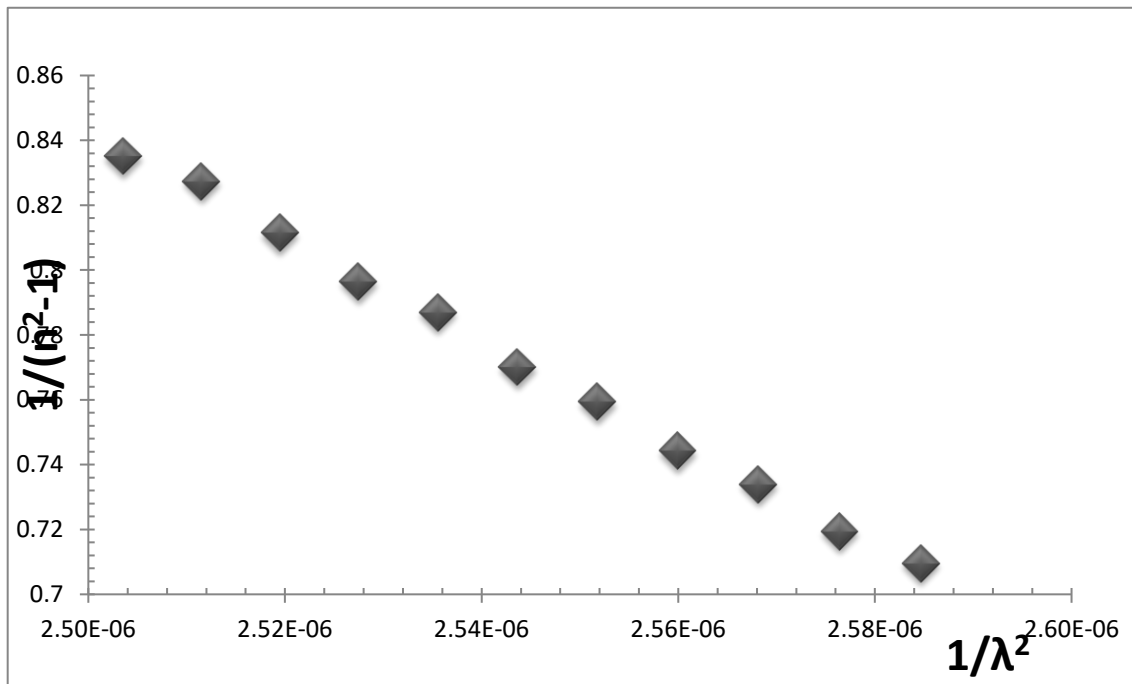


Figure (33) relationship between  $(\frac{1}{n^2-1})$  versus  $(\frac{1}{\lambda^2})$  of Co-Poly5.

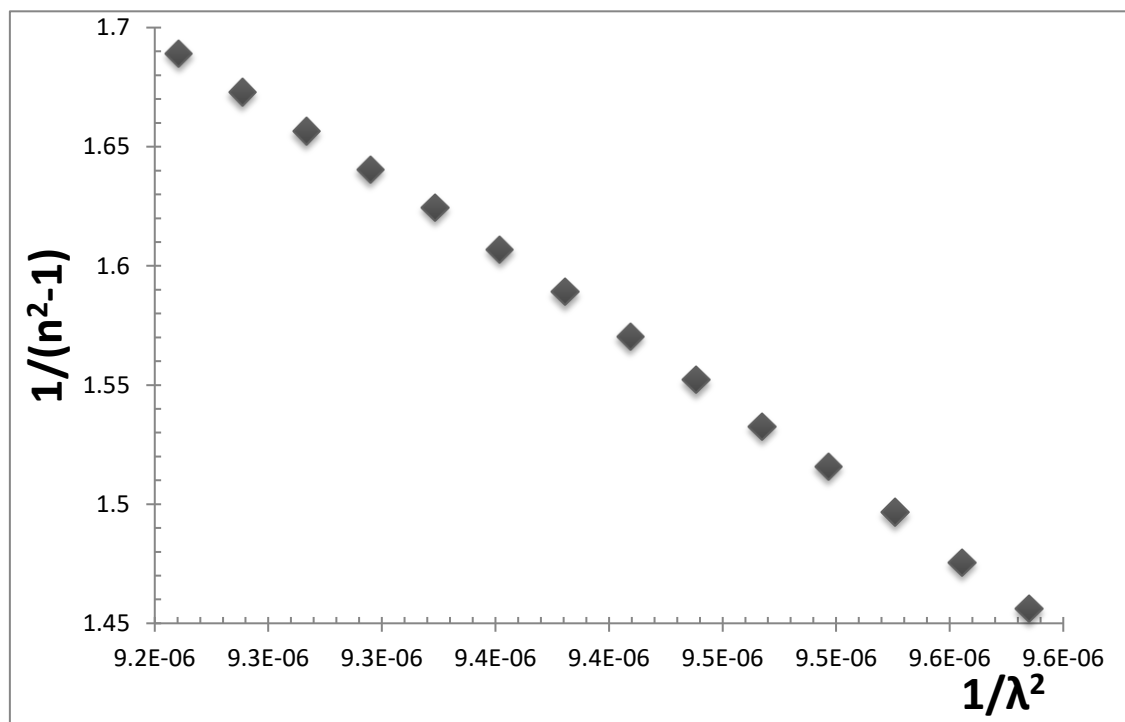


Figure (34) relationship between  $(\frac{1}{n^2-1})$  versus  $(\frac{1}{\lambda^2})$  of Co-Poly6.



Table 6: ( parameters some optical properties )

sample	Poly1	Poly2	Co-Poly3	Co-Poly4	Co-Poly5	Co-Poly6
E <sub>g</sub> (eV)	2.3	2.78	1.88	1.78	1.82	1.75
E <sub>0</sub> (ev)	2.175	1.747	0.925	1.2	0.944	1.137
E <sub>d</sub> (eV)	0.435	0.474	0.1396	0.297	0.199	1.049
n <sub>o</sub> <sup>2</sup>	1.4	1.35	1.132	1.12	1.21	1.37
ε <sub>∞</sub>	1.0954	1.271	1.07276	1.26	1.1	1.387
M-1	0.2	0.271	0.151	0.56	0.211	0.923
M-3	0.0423	0.0887	0.1765	0.576	0.2367	0.714
So	3.84 E-7	9.62 E-7	1.016 E-7	1.9 E-7	1.194 E-7	4.42 E-7
X <sup>3</sup>	1.078 E-24	1.049 E-24	2.08 E-24	2.88 E-24	2.819 E-24	0.26 E-24
λ <sub>o</sub> (nm)	1095.94	603.23	1140	1099	1326.18	914.56

## 5 :Conclusion

The study delves into enhancing polymer solar cells by incorporating Poly(3HT-co-Thio)@NPs (SiO<sub>2</sub>, ZnO, Ag) into active layers, exploring their optical properties. Analyses using XRD, SEM, FTIR, AFM, and UV-visible absorption spectroscopy revealed crystallinity in nanoparticles, varying film thicknesses, and nanoparticle-polymer interactions. Results suggest potential applications in optoelectronics. The findings emphasize the promising role of these nanoparticles in improving the efficiency of polymer solar cells, hinting at their prospective industrial utility in solar energy conversion systems.

## References

1. Chaudhary, V., Pandey, R. K., Prakash, R., Kumar, N., & Singh, A. K. (2019). Highly aligned and crystalline poly (3-hexylthiophene) thin films by off-center spin coating for high performance organic field-effect transistors. *Synthetic Metals*, **258**, 116221.
2. Liu, J., Yao, M., & Shen, L. (2019). Third generation photovoltaic cells based on photonic crystals. *Journal of Materials Chemistry C*, **7(11)**, 3121-314
3. Chen, Junwu, and Yong Cao. "Development of novel conjugated donor polymers for high-efficiency bulk-heterojunction photovoltaic devices." *Accounts of chemical research* 42.11 (2009): **1709-1718**.
4. Chen, Bo, et al. "Progress in tandem solar cells based on hybrid organic-inorganic perovskites." *Advanced Energy Materials* 7.14 (2017): **1602400**.



5. Amgar, Daniel, Sigalit Aharon, and Lioz Etgar. "Inorganic and hybrid organo-metal perovskite nanostructures: synthesis, properties, and applications." *Advanced Functional Materials* 26.47 (2016): **8576-8593**.
6. Ai, L., Shi, R., Yang, J., Zhang, K., Zhang, T., & Lu, S. (2021). Efficient combination of g-C<sub>3</sub>N<sub>4</sub> and CDs for enhanced photocatalytic performance: A review of synthesis, strategies, and applications. *Small*, **17(48)**, 2007523.
7. Joseph, I., Louis, H., Unimuke, T. O., Etim, I. S., Orosun, M. M., & Odey, J. (2020). An overview of the operational principles, light harvesting and trapping technologies, and recent advances of the dye sensitized solar cells. *Applied Solar Energy*, **56**, 334-363.
8. Monti, F., Manfredi, G., Palamà, I. E., Kovtun, A., Zangoli, M., D'Amone, S., ... & Di Maria, F. (2021). Sterilization of Semiconductive Nanomaterials: The Case of Water-Suspended Poly-3-Hexylthiophene Nanoparticles. *Advanced Healthcare Materials*, **10(6)**, 2001306.
9. Kumar, P., Dua, S., Kaur, R., Kumar, M., & Bhatt, G. (2022). A review on advancements in carbon quantum dots and their application in photovoltaics. *RSC advances*, **12(8)**, 4714-4759.
10. Ullah, S., Ferreira-Neto, E. P., Hazra, C., Parveen, R., Rojas-Mantilla, H. D., Calegaro, M. L., ... & Ribeiro, S. J. L. (2019). Broad spectrum photocatalytic system based on BiVO<sub>4</sub> and NaYbF<sub>4</sub>: Tm<sup>3+</sup> upconversion particles for environmental remediation under UV-vis-NIR illumination. *Applied Catalysis B: Environmental*, **243**, 121-135.
11. Yokozawa, Tsutomu, and Akihiro Yokoyama. "Chain-growth condensation polymerization for the synthesis of well-defined condensation polymers and  $\pi$ -conjugated polymers." *Chemical reviews* 109.11 (2009): **5595-5619**.
12. Qiu, Guo, et al. "Niobium phosphotungstates: excellent solid acid catalysts for the dehydration of fructose to 5-hydroxymethylfurfural under mild conditions." *RSC advances* 8.57 (2018): **32423-32433**.
13. Sharma, Shyamalima. "Development of polymer nanocomposite based photovoltaic devices with improved efficiency." (2016).
14. Verma, Jaya, et al. "Fabrication and testing of a multifunctional SiO<sub>2</sub>@ ZnO core-shell nanospheres incorporated polymer coating for sustainable marine transport." *Scientific Reports* 13.1 (2023): **12321**.
15. Nandiyanto, Asep Bayu Dan, Rosi Oktiani, and Risti Ragadhita. "How to read and interpret FTIR spectroscopy of organic material." *Indonesian Journal of Science and Technology* 4.1 (2019): **97-118**.
16. Hudson, Melanie. *Studies of the formation of homogeneous mixed silicon-titanium/zirconium oxides by the sol-gel route*. Diss. 1994.
17. Pryshchepa, Oleksandra, Paweł Pomastowski, and Bogusław Buszewski. "Silver nanoparticles: Synthesis, investigation techniques, and properties." *Advances in Colloid and Interface Science* 284 (2020): **102246**.



18. Liirò-Peluso, Letizia, et al. "Submolecular Resolution Imaging of P3HT: PCBM Nanostructured Films by Atomic Force Microscopy: Implications for Organic Solar Cells." *ACS applied nano materials* 5.10 (2022): **13794**-13804.
- Liirò-Peluso, Letizia, et al. "Submolecular Resolution Imaging of P3HT: PCBM Nanostructured Films by Atomic Force Microscopy: Implications for Organic Solar Cells." *ACS applied nano materials* 5.10 (2022): **13794**-13804.
19. Kuila, Biplab K., Ashesh Garai, and Arun K. Nandi. "Synthesis, optical, and electrical characterization of organically soluble silver nanoparticles and their poly (3-hexylthiophene) nanocomposites: Enhanced luminescence property in the nanocomposite thin films." *Chemistry of Materials* 19.22 (2007): **5443**-5452.
20. Gollu, Sankara Rao, et al. "Incorporation of SiO<sub>2</sub> dielectric nanoparticles for performance enhancement in P3HT: PCBM inverted organic solar cells." *Organic Electronics* 24 (2015): **43**-50.
21. Priyadharshini, R.I.; Prasannaraj, G.; Geetha, N.; Venkatachalam, P. Microwave-mediated extracellular synthesis of metallic silver and zinc oxide nanoparticles using macro-algae (*Gracilaria edulis*) extracts and its anticancer activity against human PC3 cell lines. *Appl. Biochem. Biotechnol.* 2014, **174**, 2777–2790.
22. Roy, K.; Sarkar, C.K.; Ghosh, C.K. Green synthesis of silver nanoparticles using fruit extract of *Malus domestica* and study of its antimicrobial activity. *Dig. J. Nanomater. Biostruct.* 2014, 9, **1137**–1147.
23. Zak, A. Khorsand, et al. "X-ray analysis of ZnO nanoparticles by Williamson–Hall and size–strain plot methods." *Solid State Sciences* 13.1 (2011): **251**-256.
24. Nandanwar, Ruchi, Purnima Singh, and Fozia Z. Haque. "Synthesis and characterization of SiO<sub>2</sub> nanoparticles by sol-gel process and its degradation of methylene blue." *Am. Chem. Sci. J* 5.1 (2015): 1-10.
25. Ercan, Ender, et al. "Multilevel photonic transistor memory devices based on 1D electrospun semiconducting polymer/perovskite composite nanofibers." *Advanced Materials Technologies* 6.8 (2021): **2100080**.
26. Chu, Ping-Hsun, et al. "Toward precision control of nanofiber orientation in conjugated polymer thin films: Impact on charge transport." *Chemistry of Materials* 28.24 (2016): **9099**-9109.
27. Baylan, Elif, and Ozlem Altintas Yildirim. "Highly efficient photocatalytic activity of stable manganese-doped zinc oxide (Mn: ZnO) nanofibers via electrospinning method." *Materials Science in Semiconductor Processing* 103 (2019): **104621**.
28. Mazumder, Julaiba Tahsina, et al. "First principle study on structural and optoelectronic properties and band-gap modulation in germanium incorporated tin (IV) oxide." *Materials Today Communications* 27 (2021): **102393**.
29. Kumbhakar, Partha, Chinmayee Chowde Gowda, and Chandra Sekhar Tiwary. "Advance optical properties and emerging applications of 2D materials." *Frontiers in Materials* 8 (2021): **721514**.



30. Ashery, A., A. A. M. Farag, and M. A. Shenashen. "Optical absorption and dispersion analysis based on single-oscillator model of polypyrrole (PPy) thin film." *Synthetic metals* 162.15-16 (2012): **1357**-1363.
31. Badran, Hussain A., Hussain F. Hussain, and Khalid I. Ajeel. "Nonlinear characterization of conducting polymer and electrical study for application as solar cells and its antibacterial activity." *Optik* 127.13 (2016): **5301**-5309.
32. Yakuphanoglu, F., A. Cukurovali, and I. Yilmaz. "Single-oscillator model and determination of optical constants of some optical thin film materials." *Physica B: Condensed Matter* **353**.3-4 (2004): 210-216.
33. Yakuphanoglu, F., A. Cukurovali, and I. Yilmaz. "Determination and analysis of the dispersive optical constants of some organic thin films." *Physica B: Condensed Matter* **351**.1-2 (2004): 53-58.
34. Akinwande, Deji, et al. "A review on mechanics and mechanical properties of 2D materials—Graphene and beyond." *Extreme Mechanics Letters* 13 (2017): **42**-77.

